LABORATORY SCIENCE

Aerosol and droplet creation during oscillatory motion of the microkeratome amidst COVID-19 and other infectious diseases

Pooja Khamar, MD, PhD, Rohit Shetty, MD, PhD, FRCS, Nikhil Balakrishnan, MD, Prasenjit Kabi, PhD, Durbar Roy, MTech, Saptarshi Basu, PhD, Abhijit Sinha Roy, PhD

Purpose: To quantify the atomization of liquid over the cornea during flap creation using microkeratome using high-speed shadowgraphy.

Setting: Laboratory investigational study.

Design: Laboratory study.

Method: In an experimental setup, flap creation was performed on enucleated goat's eyes (n = 8) mounted on a stand using One Use-Plus SBK Moria microkeratome (Moria SA) to assess the spread of aerosols and droplets using high-speed shadowgraphy. Two conditions were computed. A constant airflow assumed uniform air velocity throughout the room. A decaying jet assumed that local air velocity at the site of measurements was smaller than the exit velocity from the air duct.

Results: With the advancement of the microkeratome across the wet corneal surface, the atomization of a balanced salt solution was recorded on shadowgraphy. The minimum droplet size was ~90 μm. The maximum distance traversed was ~1.8 m and ~1.3 m assuming a constant airflow (setting of refractive surgery theater) and decaying jet condition (setting of an operating theater with air-handling unit), respectively.

Conclusions: The microkeratome-assisted LASIK flap creation does seem to cause spread of droplets. The droplet diameters and velocities did not permit the formation of aerosols. Therefore, the risk of transmission of the virus to the surgeon and surgical personnel due to the microkeratome procedure seems to be low.

J Cataract Refract Surg 2020; ■:1–7 Copyright © 2020 Published by Wolters Kluwer on behalf of ASCRS and ESCRS

Online Video

As of late May 2020, the COVID-19 pandemic had affected 215 countries worldwide with more than 6 million positive patients and more than 350,000 deaths.[1] Infectious disease outbreaks are challenging because they can overburden the healthcare facilities. The severe acute respiratory syndrome coronavirus 2 (SARS-CoV-2) is a viral infection caused by the new coronavirus.[2] It has rapidly become the world's 6th Public Health Emergency of International Concern.[3] The primary route of transmission of SARS-CoV-2 is through direct contact with the respiratory secretions and droplets of an infected person.[4] The virus might survive on different surfaces for days and heighten the risk of transmission.[5] Airborne transmission of a disease is defined as the transmission of infection by large droplets over short distances or through aerosols (smaller droplets) over large distances.[6,7]

Various surgical procedures performed by ophthalmologists might generate aerosols from viral shedding areas, such as the conjunctiva and tears.[8] It has been reported that the SARS-CoV-2 can be detected in the conjunctival swabs of patients with COVID-19.[9] Although there are no conclusive reports on transmission of the virus from the conjunctiva and tears, all precautions while examining and operating on patients with ophthalmic indications should be taken because many patients might be asymptomatic carriers of the virus. LASIK is one of the most commonly performed ophthalmic surgeries worldwide.[10] The LASIK flap can be created using a microkeratome that typically oscillates the blade at 6000 to 15 000 cycles per minute and produces aerosol when it comes in contact with a wet ocular surface.[11] High-frequency oscillations are known to generate aerosols.[12]

Submitted: June 9, 2020 | Final revision submitted: June 24, 2020 | Accepted: June 24, 2020

From the Department of Cornea and Refractive Surgery, Narayana Nethralaya (Khamar, Shetty, Balakrishnan), Department of Mechanical Engineering, Indian Institute of Science (Kabi, Roy, Basu), Imaging, Biomechanics and Mathematical Modeling Solutions, Narayana Nethralaya Foundation (Sinha Roy), Bangalore, India.

We would like to acknowledge the Defense Research and Development Organization, India, Chair Professorship for funding.

Corresponding author: Abhijit Sinha Roy, PhD, Narayana Nethralaya, #258/A Hosur Rd, Health City, Bommasandra, Bangalore 560099, India.
Email: asroy27@yahoo.com.

0886-3350/$ - see frontmatter
https://doi.org/10.1097/j.jcrs.0000000000000326

The droplets and aerosols can be studied using the schlieren and shadowgraph imaging technique although the former is more complicated to implement in clinical procedures such as the microkeratome. In shadowgraphy, a bright strobe LED source is used to cast the shadow of the fast-moving droplets and aerosols onto the sensor of an ultra-high-speed camera.[13,14] Therefore, we quantified the aerosol and droplet generation during flap creation using the Moria One Use-Plus SBK microkeratome (Moria SA) and assessed their trajectory using high-speed shadowgraphy and fluid mechanics principles.

METHODS

The experiment was conducted on enucleated goat eyes (n = 8) to avoid experimenting on cadaveric human eyeballs as per the guidelines laid down by the Global Eye Bank Association and Eye Bank Association of India, which prohibited retrieval of cadaveric eyes during the ongoing pandemic for the safety of healthcare personnel.[15] The goat eyes have been widely used for training and research purposes in ophthalmology.[16] The clarity of the cornea in the enucleated goat eye was inspected visually. The goat eye was inflated by injecting with a balanced salt solution (Beaver-Visitec International) through the optic nerve. After the initial preparation, the goat eye was mounted on a base such that the whole cornea, limbus, and some part of sclera were completely visible to the operating surgeon for ease of surgical maneuvering (Figure 1, A). The One Use-Plus SBK Moria microkeratome was used to create a corneal flap on the goat's eye. A standard flap of 9.0 mm in diameter and 130 μm in depth with a nasal hinge using A-1 ring was aimed. The flap creation was attempted once a vacuum of 140 mm Hg was achieved. A BSS (0.2 mL) was used to wet the corneal surface prior to flap creation (Figure 1, B). A new blade was used for each goat eye. The temperature of the experiment room was set at 21°C using a room air conditioner, and the humidity was set in the range of 40% to 50% using a dehumidifier. These settings were the same as the ones used in the operating rooms meant for refractive surgery in our hospital. Our refractive operating rooms also included room air conditioners and dehumidifier.

Shadowgraphy technique was used to visualize the droplets generated during flap creation with the microkeratome. For objects in motion, an appropriate choice of camera shutter speed was chosen to avoid blurred images. Figure 2, A shows a high-speed CCD camera (Mini UX100, Photron USA, Inc.) on the right, positioned opposite to a high-power LED source (Constellation 120, Veritas) on the left. Two sets of macrolenses were used for imaging with the camera. A 50 mm lens (Nikkor AF F1.4, Nikon Imaging Japan, Inc.) was used to visualize the trajectory of the droplets emanating from the site of incision. A 100 mm lens (ATX PRO F2.8D, Kenko Tokina Co. Ltd.) was used to image and estimate the droplet size distribution (Figure 2, B). In this case, the aperture was maintained at f/32 for maximum depth field. The surgical procedure was performed in a way such that the direction of primary trajectory of the aerosols and droplets was perpendicular to the lens camera. This allowed the trajectory to remain within the given depth of focus of the imaging system. The acquisition rate of the camera was set at 500 fps and the shutter speed at 1/18 000 seconds.

To estimate the spread of the aerosols and droplets, the size distribution was extracted from the images using the "analyze particles" plugin of ImageJ (open source image; JAVA-based image processing platform) and used for further calculations. A simple 1D analysis was used. During the course of flap cut, a droplet of diameter D μm ejected with a velocity u_d (horizontal component) was measured. Operating theaters other than the ones used for refractive surgery have high efficiency air filtration systems that create a flow of air around this droplet. Thus, the profile of the airflow might be a constant airflow (such as the refractive surgery operating theater) or a decaying jet (our other operating theaters) based on the relative positioning of the air duct and the operating table. In a decaying jet, it was assumed that the operating table was located at a horizontal distance (l_o) from the air duct. Then, the airflow velocity (u_{air}) was modeled as:

$$u_{air} = \frac{3u_{in} \times d_{duct}}{K \times l_o},\ l_o \approx \frac{3 \times d_{duct}}{K}, \quad [1]$$

where u_{in} was the exit velocity from the duct, K (~0.457) was the turbulent entrainment constant, and d_{duct} was the diameter of the duct.[17,18] Thus, equation 1 provided a measure of the local airflow velocity at the operating table. In a constant airflow scenario, u_{air} was equal to u_{in} throughout the operating room. The appropriate governing drag equation for the droplet is given below:

$$\frac{du_d}{dt} = \frac{18}{r^2}\frac{\mu_f}{\rho_d}\frac{u_{rel}(u_{air} - u_d)}{u_{rel}}, \quad [2]$$

where $u_{rel} = \sqrt{(u_{air} - u_d)^2 + v_d^2}$, $r = D/2$, v_d is the settling rate of the droplet, μ_f is the viscosity of air (18.37×10^{-6} Pa.sec), ρ_f is the density of air (1.184 kg/m^3), ρ_d is the density of droplet (997 kg/m^3), and g is the acceleration due to gravity (9.81 m/sec^2). The droplet evaporates and settles due to gravity simultaneously. The evaporation timescale can be estimated from the D^2 law, whereas the appropriate settling rate (v_d) from the Stokes equation is as follows[19]:

$$v_d = \left(\rho_d - \rho_f\right)\frac{gD^2}{18\mu_f}. \quad [3]$$

The calculation assumes that the point of surgical incision is at approximately 1 m height from the operating theater floor. Thus, the timescale of droplet settling was obtained from equation 3 as follows:

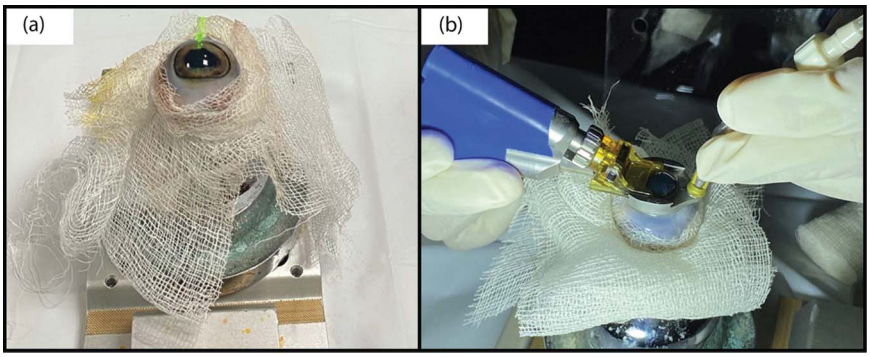

Figure 1. Experimental setup: (*A*) setup of goat's eye on a stand; (*B*) advancement of One Use-Plus SBK Moria microkeratome over the wet corneal surface.

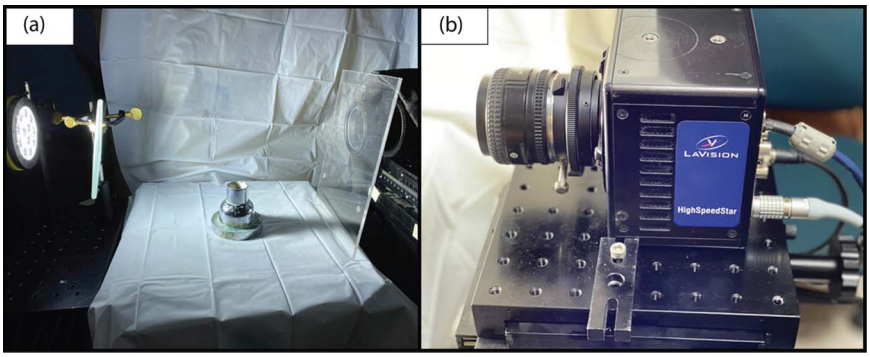

Figure 2. Imaging technique: (*A*) optical setup for high-speed shadowgraphy using CCD camera on the right and a high-power light source on the left; (*B*) the Mini-UX100 (high-speed CCD camera) coupled with a macrolens (ATX 100, 100.0 mm, f2.8D).

$$t_s = \frac{1}{v_d} = \frac{18\mu_f}{\left(\rho_d - \rho_f\right)gD}. \quad [4]$$

For the constant airflow condition, the value of u_{air} was estimated to be approximately 0.6 m/s, which was as per the certified inspection report of the operating theatres at the Narayana Nethralaya eye hospital. For the decaying jet condition, u_{in} was assumed as approximately 0.6 m/sec. The rated capacity of the air-handling units in our operating theaters (3 in number) ranged from 2364 to 2653 ft^3/min, and the number of air changes per hour was not less than 40. The properties of air at a temperature of 23°C were used in all the equations.

RESULTS

With the advancement of the microkeratome through the stroma, the atomization of water was visible on the shadowgraphy image (Figure 3, A and B) (Supplemental Digital Content 1, Video 1 in Supplementary Model, available at http://links.lww.com/JRS/A134). Most of the droplets were generated in a direction that was at an angle of 90° to the direction of advancement of the microkeratome over the cornea. Shadowgraphy in the direction of advancement of the microkeratome had technical challenges because the surgeon hands and microkeratome itself blocked the camera field of view. Figure 4, A shows the setup imaged using the 50.0 mm lens before the start of the flap cut. The droplet trajectories were visualized in Figure 4, B by superimposition of 50 sequential images. It was apparent that the smaller droplets travelled farther from the point of ejection. For example, a droplet of diameter 386 μm traveled 26.0 mm in the horizontal direction, whereas a droplet of diameter 578 μm traveled only 13.0 mm in the same direction (both measured at the same vertical depth of 0.01 m from the point of ejection). These distances were calculated assuming that there was no air circulation (ie, $u_{air} = u_{in} = 0.0$) in the theater. Given the limitation of the 50.0 mm lens in imaging the smaller droplets, a 100.0 mm lens was used for shadowgraphy as shown in Figure 4, C. The droplet size distribution was extracted from the JAVA-based image processing platform and is presented in Figure 4, D.

The most prevalent droplet diameters were in the range of 90 to 150 μm, whereas droplets larger than 500 μm were very few in numbers. We have computed the maximum traversal of a droplet based a constant airflow and decaying jet. As shown in Figure 4, E, the value of x (axial distance) showed a monotonic decrease with increasing diameter (D) of the droplet for both the conditions. Naturally, the constant airflow resulted in greater axial distance for the same droplet diameter. A power law fit showed the distance traveled by the droplets in case of a decaying jet as $x \approx 17\,604 \times D^{-2.11}$, whereas the same for constant airflow was $x \approx 52\,584 \times D^{-2.25}$. The maximum distance traversed was approximately 1.8 m and approximately 1.3 m, assuming a constant airflow (setting of refractive surgery theater) and decaying jet condition (setting of an operating theater with air-handling unit), respectively. The value of u_d used for these calculations was approximately 0.252 m/s and was estimated from the high-speed shadowgraphs.

DISCUSSION

An effective risk assessment of different surgical procedures can help mitigate the risk of transmission to healthcare

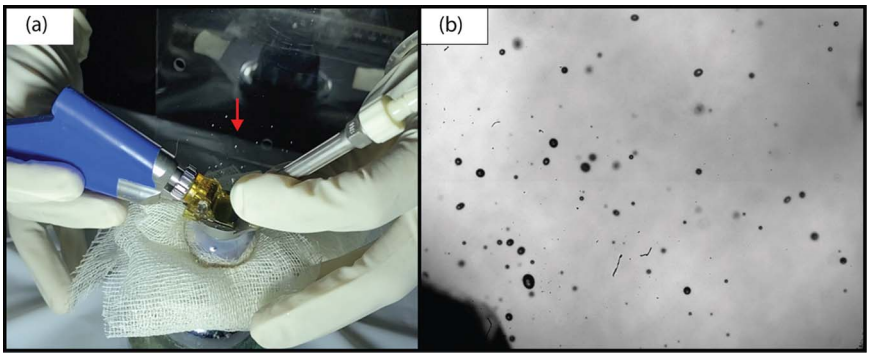

Figure 3. Clinical and shadowgraphy images of an enucleated goat eye mounted on a stand: (*A*) clinical photograph showing droplet generation on advancement of One Use-Plus SBK Moria microkeratome over the wet corneal surface; (*B*) high-speed shadowgraphy image showing shadows of droplets released during flap creation.

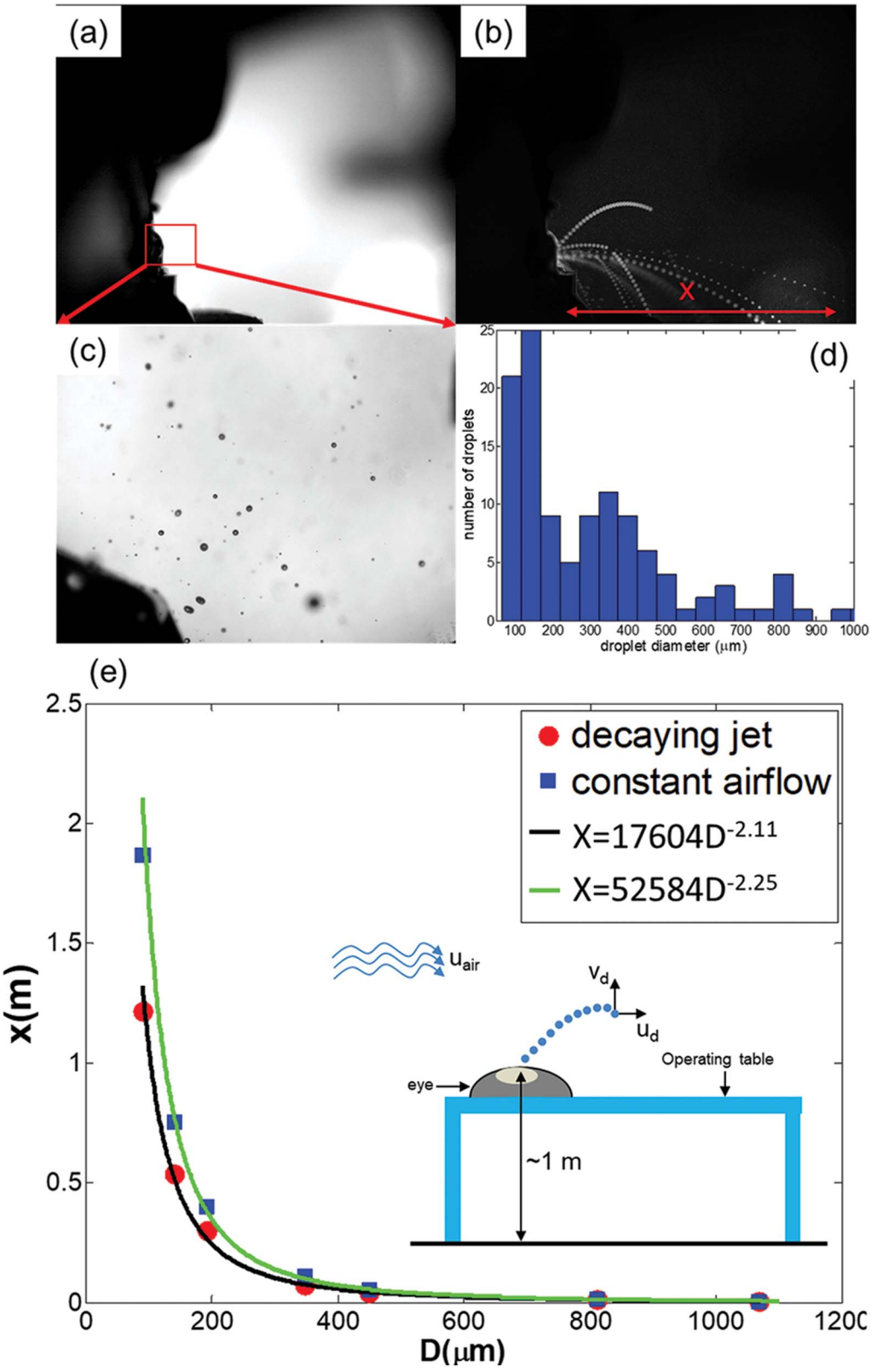

Figure 4. *A*: Side-view shadowgraph of the experimental setup before commencing the microkeratome; (*B*) superimposed images of the imaged area during the procedure illustrate the droplet trajectory. Here, *x* was the horizontal distance traveled by the droplet; (*C*) magnified image showing droplets of different sizes; (*D*) droplet size distribution presented as a histogram; (*E*) computed value of *x* from the drag equation plotted against the droplet diameter, *D* (in micrometers).

professionals. Theoretically, there is always a risk of transmission of infectious diseases through aerosols and droplets. Wong et al. and Darcy et al. demonstrated the aerosol generation in experimental models of phacoemulsification and vitrectomy, respectively.[20,21] However, the possibility of aerosol generation during LASIK flap creation has not yet been explored. The principle of shadowgraph is based on the bending of light around higher density objects (in this case, liquid droplets in air) such that the image projected on the screen (in this case, the camera sensor) is dark.[22]

Shadowgraphy when combined with imaging at a high speed (500 fps and 1/40 000 seconds of shutter speed) and with a high-resolution camera (24 μm per pixel) can capture particle sizes as small as 50 μm. It is known that droplets in the size range of 0.2 to 500 μm mostly contribute to the spread of airborne diseases.[23] Thus, it is critical to estimate the distance traveled by the ejected droplets to ascertain their potential as infection vectors. The horizontal distance (x) traveled by the droplet is dependent on both the evaporation timescales and the settling timescales and is finally determined from the smaller of the 2 quantities. Because the smallest detected droplet diameter was approximately 90 μm, the process was controlled primarily by the settling timescale. Because the smallest droplet diameter detected was greater than 24 μm, it was highly unlikely that any droplet smaller than 24 μm up to 10 μm in diameter existed because a diameter of 10 μm is usually considered as the upper limit for aerosol. However, the calculations presented in this study did not account for the clustering effect observed in sprays.[24]

In our experimental model, we used a balanced salt solution for lubricating the cornea prior to the flap creation by the microkeratome. The wetting of the corneal surface might be a contributory factor in aerosol generation. Thus, aerosol and droplet generation were observed during the advancement of the microkeratome over the corneal surface. We believe that it was due to the atomization of the balanced salt solution secondary to the oscillatory movements within the microkeratome.

Lubricating the corneal surface before use of microkeratome for flap creation is essential to prevent the epithelial erosions.[25] Thus, this might be a potential source of viral transmission from an asymptomatic patient to the operating surgeon during the procedure.

Most of the droplet diameters ranged from 90 to 900 μm during microkeratome-assisted LASIK (Figure 4, D). Droplets smaller than 90 μm were nonexistent. Although the initial size of the droplets was too large to be classified as an aerosol, subsequent viscous shear against air might reduce them to about 0.1 to 0.3 times the original size.[26] Given the droplet size distribution and their velocities, it is highly probable that they will settle on a surface before they evaporate in smaller sizes. Thus, the surgeons and other personnel in the surgical area need to take adequate measures to avoid contact with the settled droplets. It should be noted that Figure 4, E does not provide the distribution of volume of the balanced salt solution distributed over the range of droplets. Nonetheless, the larger droplets tend to settle faster, travel less distance, and have lower risk of aerosolization.

An understanding of the stochastic nature of droplet creation from the motion of the microkeratome is required. Atomization of the balanced salt solution film on the corneal surface depends on several factors, for example, frequency of oscillations, speed of advancement of the blade in the direction of flap cut, thermophysical properties of the fluid, and make of the device. Nonetheless, our experiments showed that the droplet diameters were bounded between 900 and 1200 μm in the all the captured frames of the shadowgraphy videos (Figure 4, E). For each eye, as many as 1000 frames were captured over a 2-second period. However, the distribution of the droplet sizes between the frames differed sharply because of the *stochastic* (random) nature of droplet creation in such experiments. This is a well-known phenomenon in the field of droplet fluid mechanics.[26] Thus, assessing repeatability between frames or between the eyes is physically unrealistic. We evaluated nearly 8000 frames (8 eyes) and focused on the frames that yielded the smallest droplet diameter. In this study, this diameter was 90 μm and was well within the detection limits of the system (24 μm per pixel). An example of such a droplet distribution was provided in Figure 4, E.

The iPhone video showed that direct visualization of droplets through surgical microscope or with the naked eye was possible during the advancement of the microkeratome. However, the quantification of the spread distances, droplet diameters, and presence of aerosols cannot be performed from the iPhone video itself. However, the minimum viral load required in aerosols to cause a successful transmission of COVID-19 has not been established. Theoretically, even a single virus might be sufficient to transmit a respiratory infection.[27] The excimer laser ablation plume did not seem to transmit the human immunodeficiency virus, herpes virus, and varicella zoster virus because they did not seem to survive the ablation.[28,29] Furthermore, there is no report confirming the presence of SARS-CoV-2 in the excimer laser plume and consequently its transmission. Therefore, the SARS-CoV-2 seems unlikely to pose a health hazard through laser ablation in LASIK and SMILE. Furthermore, femtosecond laser flap creation is a safer alternative to microkeratome because there are no oscillating blades involved. In addition, the results of this study applied to all infectious diseases that have the potential to be transmitted through aerosols and droplets.

After ablation in photorefractive keratectomy and application of mitomycin, slow washing of the surface with a balanced salt solution is recommended because this might lead to droplets/aerosol formation. This needs to be evaluated in future studies. Topical povidone–iodine drops prior to LASIK for a contact period of 2 minutes can reduce the effectivity of the SARS-CoV-2 virus below detectable levels.[30] In conclusions, microkeratome-assisted LASIK flap creation resulted in generation of droplets. However, it would be too premature to confirm its role in the transmission of the SARS-CoV-2 virus. Although most of the refractive surgery patients belong to the younger age group who might have less mortality, they are more likely to be asymptomatic carriers of the virus.[31] Thus, precautions such as face mask on the surgeon and patient, use of Betadine as a potent antiviral and bacterial disinfectant prior to the surgery, and use of a protective shield between the surgical area and personnel to reduce the risk of transmission, if at all present, should be strictly followed.[21] A limitation of the study was the 2D nature of analyses. A more refined 3D analysis of the droplet trajectories might

shed more light on the physics of droplet creation by the microkeratome. Another limitation was that only 1 model of microkeratome was tested because this was the only model available in our hospital, and different makes might have different oscillatory settings.

WHAT WAS KNOWN

- The severe acute respiratory syndrome coronavirus 2 virus can spread through aerosols and droplets.
- In ophthalmology, procedures that might have the propensity to create aerosols and droplets exist.

WHAT THIS PAPER ADDS

- As the microkeratome oscillated during the flap cut, large droplets measuring greater than 90 μm were created. These droplets could travel up to distances of 1.8 m.
- However, the droplets were too large and will settle down on surface before aerosolization could occur, and the risk of aerosolization and transmission through these droplets was very low.
- Adequate precautions should be followed during flap cut with microkeratome.

REFERENCES

1. Available at: https://www.worldometers.info/coronavirus/. Accessed May 30, 2020
2. Astuti I, Ysrafil. Severe acute respiratory syndrome coronavirus 2 (SARS-CoV-2): an overview of viral structure and host response. Diabetes Metab Syndr 2020;14:407–412
3. World Health Organization. Statement on the second meeting of the International Health Regulations (2005). Emergency Committee regarding the outbreak of novel coronavirus (2019-nCoV). Available at: https://www.who.int/news- room/detail/30-01-2020-statement-on-the-second-meeting-of-the- international-health-regulations-(2005)-emergency-committee-regarding-the-outbreak-of-novel-coronavirus-(2019ncov). Accessed May16, 2020
4. Li Q, Guan X, Wu P, Wang X, Zhou L, Tong Y, Ren R, Leung KSM, Lau EHY, Wong JY, Xing X, Xiang N, Wu Y, Li C, Chen Q, Li D, Liu T, Zhao J, Liu M, Tu W, Chen C, Jin L, Yang R, Wang Q, Zhou S, Wang R, Liu H, Luo Y, Liu Y, Shao G, Li H, Tao Z, Yang Y, Deng Z, Liu B, Ma Z, Zhang Y, Shi G, Lam TTY, Wu JT, Gao GF, Cowling BJ, Yang B, Leung GM, Feng Z. Early transmission dynamics in Wuhan, China, of novel coronavirus-infected pneumonia. N Engl J Med 2020;382:1199–1207
5. van Doremalen N, Bushmaker T, Morris DH, Halbrook MG, Gamble A, Williamson BN, Tamin A, Harcourt JL, Thornburg NJ, Gerber SI, Lloyd-Smith JO, de Wit E, Munster VJ. Aerosol and surface stability of SARS-CoV-2 as compared with SARS-CoV-1. N Engl J Med 2020;382:1564–1567
6. Tellier R, Li Y, Cowling BJ, Tang JW. Recognition of aerosol transmission of infectious agents: a commentary. BMC Infect Dis 2019;19:101
7. Jones RM, Brosseau LM. Aerosol transmission of infectious disease. J Occup Environ Med 2015;57:501–508
8. Lu CW, Liu XF, Jia ZF. 2019-nCoV transmission through the ocular surface must not be ignored. Lancet 2020;395:e39
9. Kumar K, Prakash AA, Gangasagara SB, Rathod SBL, Ravi K, Rangaiah A, Shankar SM, Basawarajappa SG, Bhushan S, Neeraja TG, Khandenahalli S, Swetha M, Gupta P, Sampritha UC, Prasad GNS, Jayanthi CR. Presence of viral RNA of SARS-CoV-2 in conjunctival swab specimens of COVID-19 patients. Indian J Ophthalmol 2020;68:1015–1017
10. Statista. Number of LASIK Surgeries in the United States from 1996 to 2020. Statista; 2019. Available at: https://www.statista.com/statistics/271478/number-of-lasik-surgeries-in-the-us/. Accessed May 30, 2020
11. Tasman W, Jaeger EA. Duane's Ophthalmology. Philadelphia: Lippincott Williams & Wilkins; 2009
12. Fang TP, Lin HL, Chiu SH, Wang SH, DiBlasi RM, Tsai YH, Fink JB. Aerosol delivery using jet nebulizer and vibrating mesh nebulizer during high frequency oscillatory ventilation: an in vitro comparison. J Aerosol Med Pulm Drug Deliv 2016;29:447–453
13. Tang JW-T, Settles G. Images in clinical medicine: coughing and masks. N Engl J Med 2009;361:e62
14. Tang JW, Liebner TJ, Craven BA, Settles GS. A schlieren optical study of the human cough with and without wearing masks for aerosol infection control. J R Soc Interf 2009;6(suppl 6):S727–S736
15. Global Alliance of Eye Bank Associations. Alert up-date: coronavirus (COVID-2019) and ocular tissue donation. Available at: http://www.gaeba.org/wpcontent/uploads/2020/03/EBAI_COVID-19-Guidelines_21032020.pdf. Accessed Nay 22, 2020
16. Sengupta S, Dhanapal P, Nath M, Haripriya A, Venkatesh R. Goat's eye integrated with a human cataractous lens: a training model for phacoemulsification. Indian J Ophthalmol 2015;63:275–277
17. Abania N, Reitz RD. Unsteady turbulent round jets and vortex motion. Phys Fluids 2007;19:125102
18. Schlichting H, Gersten K. Boundary Layer Theory. 8th ed. Berlin/Heidelberg, Germany: Springer-Verlag; 2017
19. Sirignano WA. Fluid Dynamics and Transport of Droplets and Sprays. Cambridge, United Kingdom: Cambridge University Press; 1999
20. Wong RS, Banerjee P, Kumaran N. Aerosol generated procedure in intraocular surgery. Available at: https://www.youtube.com/watch?v=0pjkNFwIHCA. Accessed May 28, 2020
21. Darcy K, Elhaddad O, Achiron A, Keller J, Leadbetter D, Tole D, Liyanage S. Aerosol during phaco (cataract surgery): how to make cataract surgery safe during Covid-19. Available at: https://www.youtube.com/watch?v=8LGwI9LIYmU&feature=youtu.be. Accessed May 22, 2020
22. Tropea C, Yarin A, Foss JS. Handbook of Experimental Fluid Mechanics. Berlin/Heidelberg, Germany: Springer-Verlag; 2007
23. Gralton J, Tovey E, McLaws ML, Rawlinson WD. The role of particle size in aerosolised pathogen transmission: a review. J Infect 2011;62:1–13
24. Manish M, Sahu S. Analysis of droplet clustering in air-assist sprays using Voronoi tessellations. Phys Fluids 2018;30:123305
25. Wilkinson PS, Davis EA, Hardten DR. LASIK. Ophthalmology. 3rd ed. Missouri: Mosby; 2008
26. Chaudhuri S, Basu S, Kabi P, Unni V, Saha A. Modeling the role of respiratory droplets in Covid-19 type pandemics. Phys Fluid (1994) 2020;32:063309
27. Nicas M, Nazaroff WW, Hubbard A. Toward understanding the risk of secondary airborne infection: emission of respirable pathogens. J Occup Environ Hyg 2005;2:143–154
28. Taravella MJ, Weinberg A, Blackburn P, May M. Do intact viral particles survive excimer laser ablation? Arch Ophthalmol 1997;115:1028–1030
29. Hagen KB, Kettering JD, Aprecio RM, Beltran F, Maloney RK. Lack of virus transmission by the excimer laser plume. Am J Ophthalmol 1997;124:206–211
30. Kariwa H, Fujii N, Takashima I. Inactivation of SARS coronavirus by means of povidone-iodine, physical conditions and chemical reagents. Dermatology 2006;212(suppl 1):119–123
31. Hospitalization rates and characteristics of patients hospitalized with laboratory-confirmed coronavirus disease 2019—COVID-NET, 14 states, March 1–30, 2020. Available at: https://www.cdc.gov/mmwr/volumes/69/wr/mm6915e3.htm. Accessed June 23, 2020

Disclosures: *None of the authors has a financial or proprietary interest in any material or method mentioned.*

000 Aerosol and droplet creation during oscillatory motion of the microkeratome amidst COVID-19 and other infectious diseases

Pooja Khamar, MD, PhD, Rohit Shetty, MD, PhD, FRCS, Nikhil Balakrishnan, MD, Prasenjit Kabi, PhD, Durbar Roy, MTech, Saptarshi Basu, PhD, Abhijit Sinha Roy, PhD

High-speed shadowgraphy showed droplets generated during flap cut with microkeratome. However, aerosolization of these droplets was unlikely because these droplets would settle on surface before aerosolization.